Earthquake Engineering, Tenth World Conference © 1992 Balkema, Rotterdam. ISBN 90 5410 060 5

Spatial variation study on earthquake ground motion observed by the Chiba array

Fumio Yamazaki & Turgay Türker
Institute of Industrial Science, University of Tokyo, Japan

ABSTRACT: Using earthquake ground motion recorded by a dense three-dimensional array in Chiba, Japan, the wavenumber spectrum was calculated for various frequency ranges. A wavenumber spectrum model was constructed to fit the observed wavenumber spectrum. The model was used to demonstrate the spatial correlation characteristics of earthquake ground motion in terms of the space-time cross-spectral density function and the spatial coherence function. Since the proposed model was made to be non-quadrant symmetric with respect to the wavenumber axes, the model can represent propagating seismic waves having dominant apparent velocity and azimuthal angle.

1 INTRODUCTION

Spatial variation of earthquake ground motion is one of the important issues to be considered in the seismic design of spatially extended structures. The frequency-wavenumber (FK) power spectrum can fully describe seismic waves which propagate coherently through a site. To obtain the exact FK spectrum in the three-dimensional (3D) space (2D in space and 1D in time), time histories at equi-spaced grid points are generally required. However, this is not practical in actual array observations. Hence, a weighted sum over the station points is usually employed instead of a spatial integral. Then, the two-dimensional wavenumber power spectrum can be estimated for a specified frequency range. The conventional method and high-resolution method have been developed and widely used for the analysis of array records (Abrahamson and Bolt, 1987). The azimuth and velocity of seismic waves in a certain frequency range were identified based on the obtained wavenumber spectra (e.g., Bolt et al., 1982).

Once an FK spectrum is obtained, it can be used for simulation of stochastic waves. For this purpose, attempts to construct analytical forms of the FK spectrum have started. Deodatis et al. (1990a) recently proposed an analytical 3D FK spectrum model that assumes a point source and quadrant symmetry. This model can be applied to a large space including a source. For a space of local array size, Harada (1991) proposed an analytical 3D FK spectrum model which considers spatial variation of local soil parameters. This model explained the tendency of the FK spectrum obtained from the SMART-1 array. However, more observed data may be required to test the validity of these analytical models.

To provide further information on observed FK spectra, earthquake records obtained by the Chiba array (Katayama et al., 1990) are employed in this study. An FK spectrum analysis is conducted for an event and an analytical 3D FK spectrum model is constructed using the observed one as a target. The model is made to be non-quadrant symmetric to represent propagating seismic waves with dominant direction and velocity. The FK spectrum model is further utilized to evaluate spatial correlation characteristics in terms of the space-time cross-spectral density function and the spatial coherence function.

2 THE CHIBA SEISMOMETER ARRAY AND THE 1985 SOUTH IBARAGI EVENT

Figure 1 shows the layout of the Chiba array, which has 15 boreholes with 44 piezoelectric type accelerometers installed at several depths. In this study, records from 15 accelerometers at -1m from the ground level (GL -1m) are used. Note that four boreholes which are 5m apart from borehole C0 are not shown in the figure. Topographical and geological conditions of the site are generally simple and the ground surface is almost flat.

In this array, more than 160 earthquake events have been successfully recorded since the start of the observation in 1982. A strong motion database comprising major 27 events has been created recently.

For this study, the South Ibaragi Prefecture earthquake, which occurred on October 4, 1985, was selected. Its magnitude was 6.1 in JMA scale and its focal depth was 78km. The epicenter was 28km from the array in the N9°E direction. The event generated one of the second strongest ground motions at the Chiba array site. Figure 2 shows the nonstationary spectrum for the EW-component recorded at GL -1m in borehole C0. Note that the EW-direction is close to the transverse-direction. The arrival of the P-wave is seen at about 0s and that of the S-wave at about 11s. Time dependency of frequency contents is slightly observed.

3 WAVENUMBER SPECTRUM FOR THE 1985 SOUTH IBARAGI EVENT

For the EW-component of the 1985 South Ibaragi Prefecture event, the wavenumber spectra were computed using the high-resolution scheme. The Parzen window with a window width of 0.4Hz was employed

for frequency-filtering the records. The time segment t =11-21s, which corresponds to the S-wave, was used. The time interval was taken as Δt =0.005s with the total number of intervals N=4,096.

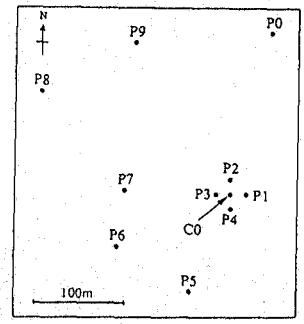

Figure 1. Layout of the Chiba array

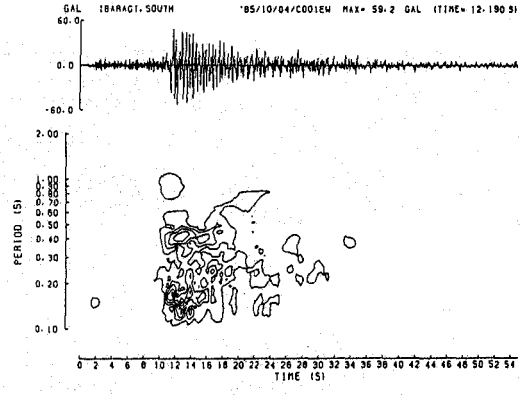

Figure 2. Nonstationary spectrum for the EW-component of the 1985 South Ibaragi earthquake at C001

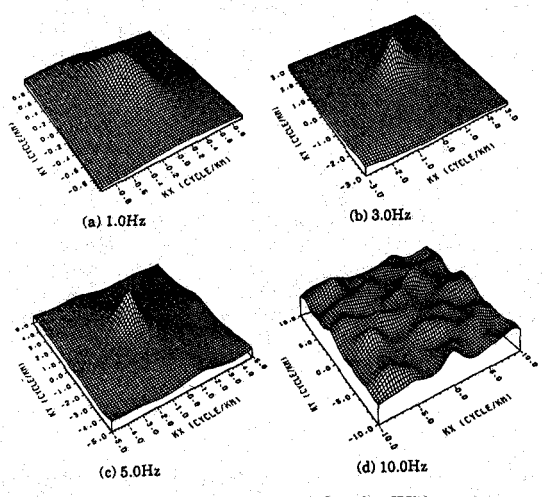

Figure 3. Wavenumber spectra for the EW-component of the South Ibaragi event at 4 frequency windows

Figure 3 shows the wavenumber power spectra for the filtered waves of the EW-component having center frequencies about 1.0, 3.0, 5.0, and 10.0Hz. Clear peaks, which indicate the azimuth and slowness of coherently propagating waves, are seen in the k_x-k_y plane. The slowness, s, can be obtained from the wavenumber vector as

$$s = \sqrt{k_x^2 + k_y^2} / f_c \qquad (1)$$

where f_c is the center frequency of the Parzen window. The slowness is set at 1 km/s at the four corners of all the plots. The apparent velocity, c, can be obtained by taking the inverse of the slowness as $c = 1/s$. The maximum peak in each plot is scaled to have unit amplitude. It is noticed that no clear peak exists at f_c =10Hz. This fact shows that the horizontal component becomes spatially random in the high frequency range.

A seismic wave is usually assumed to be a sum of signal and noise components. The volume of the dominant peak in the wavenumber plot corresponds to the power of signal while the volume of the base portion represents that of noise. The noise ratio is seen to increase with frequency.

To observe the effect of directivity on wavenumber spectra, the FK spectrum analysis was further conducted for six horizontal directions obtained by coordinate rotation. For the selected time segment, this analysis was made for center frequencies between 0.39Hz and 8.0Hz with approximately 0.1Hz interval. The azimuthal angles and apparent velocities obtained by the analysis for the six directions are shown in Figures 4 and 5, respectively. The azimuthal angles were generally close to the epicentral direction (N9°E) and fluctuating parts mostly corresponded to frequency contents having small power. Variation of the azimuthal angle with respect to the six directions was also seen to be rather small.

The apparent velocities were mostly in the range of 4-6 km/s for the six directions and the fluctuations also corresponded to frequencies of small power. Since the shear wave velocity of the top soil layer is 140m/s by a geophysical exploration, the incident angle of the horizontal motion is considered to be almost normal to the ground surface. By integrating the wavenumber power spectra over the wavenumber axes, the power spectra for the six directions were obtained. The power spectra are also close to one another as shown in Figure 6.

4 MODELING OF FREQUENCY-WAVENUMBER POWER SPECTRUM

The wavenumber power spectrum $S(k_x,k_y|f=f_C)$ obtained for a selected center frequency f_C is useful in identifying wave types and their characteristics. By moving the center frequency continuously, the three-dimensional frequency-wavenumber (FK) power spectrum $S(k_x, k_y, f)$ can be obtained. Such a 3D FK spectrum can fully describe spatially varying earthquake ground motion. Hence, an analytical FK spectrum model is sought considering its engineering use.

Assuming a space-time process $u(x, y, t)$ is stationary in time, homogeneous in space, and ergodic in both, the following 3D FK spectral density function is considered:

$$S(k_x,k_y,f) = S(f)\,A(k_x,k_y|f) \qquad (2)$$

where $S(f)$ is the two-sided power spectral density function and $A(k_x, k_y|f)$ is the normalized conditional wavenumber spectrum at frequency f. The two-fold integration of A over the wavenumbers is unity

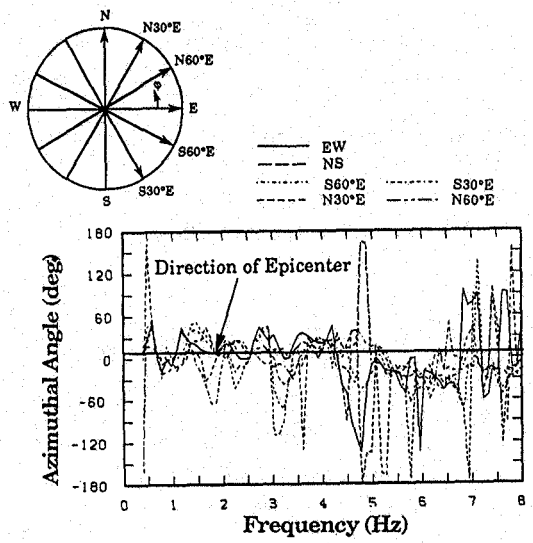

Figure 4. Variation of azimuthal angles obtained from the FK spectra for the six directions

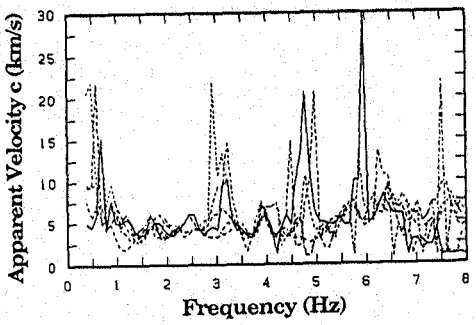

Figure 5. Variation of apparent velocities obtained from the FK spectra for the six directions

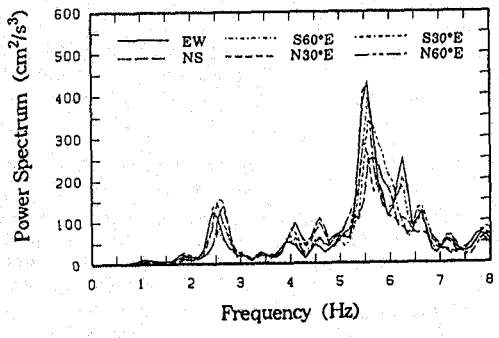

Figure 6. Comparison of power spectra obtained from the integration of the FK spectra for the six directions

regardless of frequency f.

To describe this wavenumber spectrum in the 2D wavenumber space, two more coordinate systems shown in Figure 7 are introduced. The first transformed coordinate system $\mathbf{k}^*=[k^*_x, k^*_y]^T$ can be obtained by the rotation of the original coordinate $\mathbf{k}=[k_x, k_y]^T$ by angle φ:

$$\mathbf{k}^* = \mathbf{T}\,\mathbf{k} \tag{3}$$

where $\mathbf{T}$ is the coordinate rotation matrix. The second coordinate transform is the shift of the origin from point O to point P in Figure 7. The new coordinate system $\mathbf{k}'=[k'_x, k'_y]^T$ is represented by

$$\mathbf{k}' = \mathbf{k}^* - \mathbf{k}^*_0 = \mathbf{T}(\mathbf{k} - \mathbf{k}_0) \tag{4}$$

where $\mathbf{k}_0$ and $\mathbf{k}^*_0$ denote the position of the origin P of $\mathbf{k}'$ coordinate in terms of the respective coordinates.

For the 2D wavenumber spectrum, an anisotropic exponential function is assumed using the $\mathbf{k}'$ coordinate:

$$A(k'_x, k'_y|f) = \frac{\alpha_x\alpha_y}{\pi}\exp\left[-(\alpha_x k'_x)^2-(\alpha_y k'_y)^2\right] \tag{5}$$

where α_x and α_y are parameters with the dimension of length and are expressed as functions of frequency. For a fixed frequency, this model possesses an ellipsoidal correlation structure with k'_x being the long axis.

The peak location of this FK spectrum model represents dominant apparent velocity, c, and azimuthal angle, θ, as follows:

$$|\mathbf{k}_0| = |\mathbf{k}^*_0| = \frac{f}{c} \quad ; \quad \theta = \tan^{-1}\left(\frac{k_{x0}}{k_{y0}}\right) \tag{6}$$

where θ is defined clockwise from the north (k_y). As depicted in Figure 7, $\Omega(=\pi/2-\theta)$ is the rotation angle of axis k_x' from the north. These two angles, Ω and θ, exhibit some differences in the actual wavenumber spectra. However, in such cases, the direction of wave propagation and the principal axis of wave coherency become different. Since it is difficult to consider such a state for homogeneous soil media, $\Omega=\theta$ may be assumed. This assumption indicates that the wavenumber spectrum is symmetric with respect to the radial and transverse directions and that coherence is stronger in the transverse direction than in the radial direction.

Since the model does not employ a quadrant symmetry

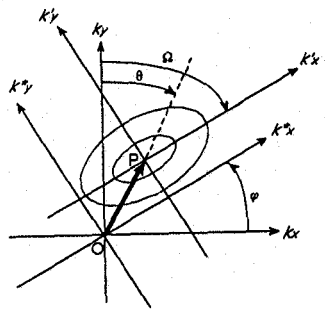

Figure 7. Wavenumber spectrum model and three coordinate systems

assumption with respect to the original wavenumber axes, it can deal with propagating waves having dominant directivity. This kind of modeling may be necessary to represent spatial variation of earthquake ground motion observed by seismic arrays. On the contrary, the FK spectrum model with quadrant symmetry considers purely stochastic ground motion with no dominant propagation direction.

The frequency-dependent parameters, α_x and α_y, control the shape of the wavenumber spectrum at each frequency, and the following functional forms are currently considered:

$$\alpha_x(f) = a_1 \exp(-f^{a_2} + a_3 f)$$
$$\alpha_y(f) = b_1 \exp(-f^{b_2} + b_3 f) \qquad (7)$$

where a_1, a_2, a_3, b_1, b_2 and b_3 are coefficients to be determined by applying the least squares method.

5 DETERMINATION OF SHAPE PARAMETERS

Using the observed wavenumber spectra for the 1985 South Ibaragi event, the parameters of the proposed 3D FK spectrum model were determined. The observed 2D wavenumber spectra were selected as a target at 12 discrete center frequencies between 0.39Hz and 7.03Hz with 0.59Hz interval. The two parameters, α_x and α_y, at each frequency were determined separately by taking a least squares fitting of sections of the observed wavenumber spectrum on axes k_x' and k_y'. As shown in Figure 8, the observed wavenumber spectrum was first normalized to have unit height at the peak. The sections of this normalized wavenumber spectrum were then plotted along the axes k_x' and k_y' as shown by small circles in Figure 9. The α_x and α_y values at this frequency were then sought by the least squares method. The section of the model using the resultant α_x is also shown by solid lines in Figure 9. Since there is only one parameter to fit for each wavenumber axis, the fitting of the model to the observed spectrum has limitation.

This procedure was conducted for the 12 discrete center frequencies and the obtained α_x is plotted by symbols in Figure 10. To get continuous functions of them, the least squares method was again employed. The six constants in Eq. 7 were then obtained, and the resultant model of $\alpha_x(f)$ is also depicted in Figure 10.

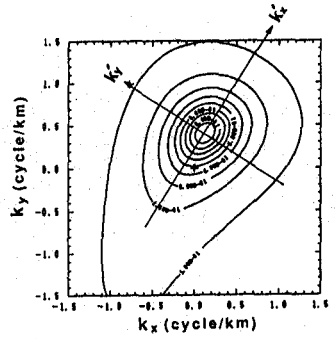

Figure 8. Observed wavenumber spectrum for the South Ibaragi event at f =1.5Hz

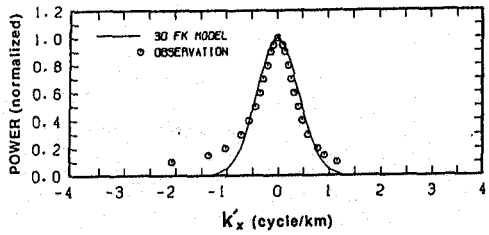

Figure 9. Section of the normalized 2D wavenumber spectrum at f =1.5Hz

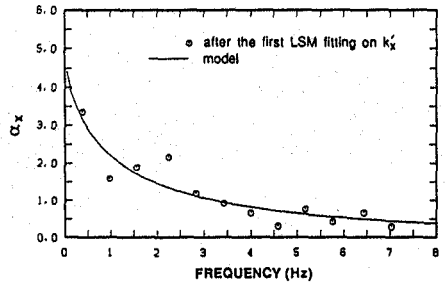

Figure 10. Variation of observed and modeled shape parameter α_x with frequency

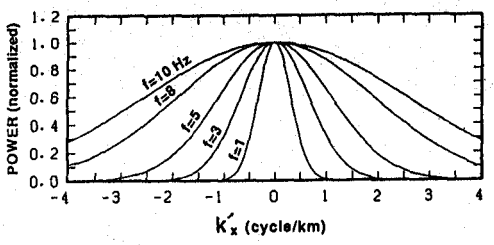

Figure 11. Normalized shapes of the wavenumber spectrum model at several frequencies

Using the continuous functions of the shape parameters, Figure 11 compares the normalized shapes of the analytical wavenumber spectra for various frequencies. From the figure, the concentration of power is seen in narrow wavenumber ranges for low frequencies while the power spreads over wide wavenumber ranges for high frequencies. Thus, in this model, earthquake ground motion is more coherent in low frequency contents than in high frequency contents, which is consistent with actual observations.

6 SPATIAL CORRELATION ANALYSIS

The frequency-wavenumber power spectrum can fully describe wave fields and it is directly applicable for the simulation of stochastic waves (Deodatis et al., 1990b; Türker and Yamazaki, 1991). However, equivalent but different representations (Vanmarcke, 1983) of second-order statistics are also often utilized. Because the three-dimensional FK spectrum, $S(\mathbf{k}, f)$, is a function of two wavenumbers and frequency, several versions of its

Fourier transform exist. If a two-fold Fourier transform with respect to the wavenumbers is taken, the space-time cross-spectral density function $C(\xi, f)$ can be obtained:

$$C(\xi, f) = \int_{-\infty}^{\infty} S(\mathbf{k}, f) \exp\left[2\pi i\, \xi \cdot \mathbf{k}\right] d\mathbf{k} \qquad (8)$$

where $\xi=[\xi_x, \xi_y]^T$ is the separation vector. The cross-spectral density function C is generally complex. When the FK spectrum $S(\mathbf{k}, f)$ is quadrant symmetric with respect to wavenumber axes k_x and k_y, $C(\xi, f)$ becomes a real function.

It is interesting to observe the shape of $C(\xi, f)$ when $S(\mathbf{k}, f)$ is given. For the FK spectrum model defined by Eqs. 2 and 5, the analytical Fourier transform can be carried out. To do this, $\mathbf{k}^*$ coordinate in Figure 7 is used instead of $\mathbf{k}$ coordinate. The corresponding space lag vector is also replaced by $\xi^*=[\xi^*_x, \xi^*_y]^T$, which can be obtained by the same coordinate rotation in Eq. 3. It is rather obvious that Eq. 8 is still valid for other Cartesian coordinates. Thus, the following relationship exists for the set of wavenumber vector $\mathbf{k}^*$ and space lag vector ξ^*:

$$C(\xi^*, f) = \int_{-\infty}^{\infty} S(\mathbf{k}^*, f) \exp\left[2\pi i\, \xi^* \cdot \mathbf{k}^*\right] d\mathbf{k}^* \qquad (9)$$

To perform the analytical Fourier transform for the function given by Eq. 5, one more coordinate transform is necessary. The coordinate translation given by Eq. 4 is introduced in Eq. 9. Replacing $\mathbf{k}^*$ by $\mathbf{k}'+\mathbf{k}^*_0$ gives

$$C(\xi^*, f) = \int_{-\infty}^{\infty} S(\mathbf{k}^*, f) \exp\left[2\pi i\, \xi^* \cdot (\mathbf{k}'+\mathbf{k}^*_0)\right] d\mathbf{k}'$$

$$= \int_{-\infty}^{\infty} S(\mathbf{k}', f) \exp\left[2\pi i\, \xi^* \cdot \mathbf{k}'\right] d\mathbf{k}' \times \exp\left[2\pi i\, \xi^* \cdot \mathbf{k}^*_0\right] \qquad (10)$$

Note that $\xi'=\xi^*$. The first term of the left side of Eq. 10 is the two-fold Fourier transform of $S(\mathbf{k}', f)$. This integration becomes a real value when $S(\mathbf{k}', f)$ is quadrant symmetric with respect to $\mathbf{k}'$ coordinate. In the present case, $S(\mathbf{k}', f)$ is quadrant symmetric and analytically integrable. The second term of the left side of Eq. 10 is a complex number which reflects the phase difference between two points with the separation ξ^*. Considering the relationship given by Eq. 6, the second term can be rewritten as the ordinary plane wave having speed c. Then, Equation 10 becomes

$$C(\xi', f) = S(f) \exp\left[-\left(\frac{\xi'_x}{\alpha_x}\right)^2 - \left(\frac{\xi'_y}{\alpha_y}\right)^2\right] \times \exp\left[2\pi f i \left(\frac{\xi' \cdot \mathbf{a}}{c}\right)\right] \qquad (11)$$

where $\mathbf{a}$ is the directional cosine vector of $\mathbf{k}^*_0$ and indicates the wave propagation direction. It is easy to see that $C(\xi', f)$ is a product of the amplitude function and the phase function. Hence, this cross-spectral density function is described by the closed form and has basically the same form as those proposed by Loh (1985) and Harichandran and Vanmarcke (1986).

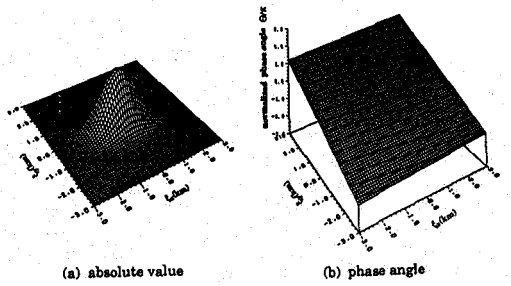

(a) absolute value (b) phase angle

Figure 12. Absolute value and phase angle of the space-time cross-spectral density function model at f =1.5Hz

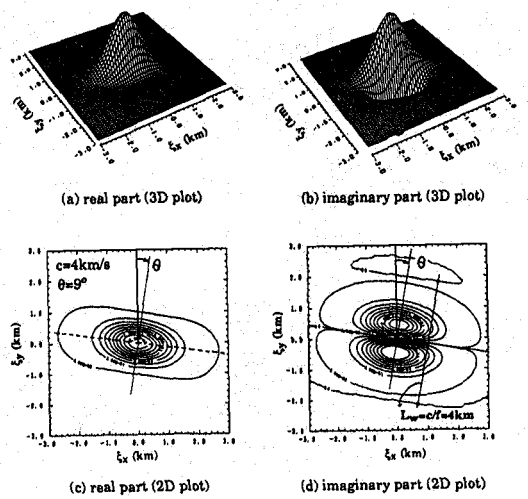

(a) real part (3D plot) (b) imaginary part (3D plot)

(c) real part (2D plot) (d) imaginary part (2D plot)

Figure 13. Real and imaginary parts of the space-time cross-spectral density function model at f =1.5Hz

It is obvious, however, that the two-fold Fourier transform in Eq. 8 can be performed numerically with the aid of the Fast Fourier transform algorithm. The example shown below uses this numerical technique.

For the FK spectrum model represented by Eqs. 2 and 5, the cross-spectral density function $C(\xi, f)$ is calculated for the fixed frequency f =1.0Hz. Figure 12 shows the absolute value and phase angle of $C(\xi, f)$ while Figure 13 plots the real and imaginary parts of the same value. Apparent velocity, c=4.0km/s, and azimuthal angle, θ=9°, were used for the model. In both figures, the target azimuthal direction can be observed. The apparent wave length (L_w =1/k =c/f) can also be observed as the distance corresponding to the phase difference of 2π in Figure 12 (b) or as the separation between zero-crossing lines in Figure 13 (d).

The normalized form of the space-time cross-spectral density function is often used as the measure of coherency in space-time processes. The coherence function is the square of the modulus of the coherency as

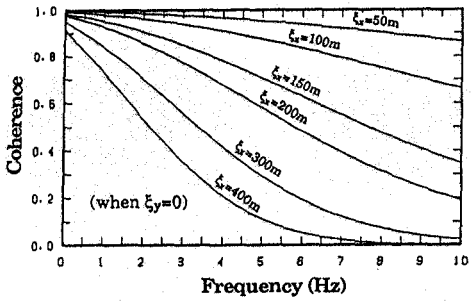

Figure 14. Coherence function models for the South Ibaragi event at several fixed separation distances

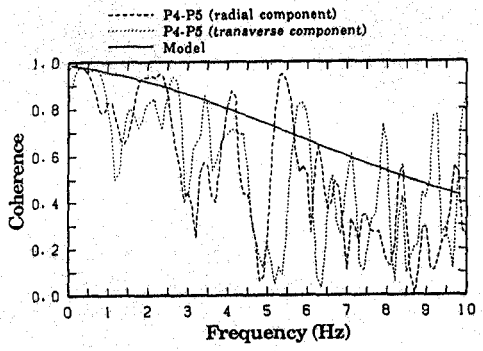

Figure 15. Comparison of the observed and modeled coherence functions between P4 and P5 points for the South Ibaragi event (ξ_x=45.1m, ξ_y=100.4m, ξ=110.1m)

$$|\gamma(\xi, f)|^2 = \frac{|C(\xi, f)|^2}{S^2(f)} \qquad (12)$$

For $C(\xi', f)$ given by Eq. 11, the coherence function can be obtained easily in the closed form. The coherence functions $|\gamma(f|\ \xi=\xi_i)|^2$ for fixed separation distances are shown as functions of frequency in Figure 14. The loss of coherence is clearly seen with the increase of the separation and the frequency, which is seen in actual array observations.

Figure 15 compares the coherence model obtained by the above procedure and the ordinary two-point coherence calculated from the 1985 South Ibaragi records. Agreement is seen between the model and observed coherences.

7 CONCLUSIONS

Using the Chiba array records from the 1985 South Ibaragi Prefecture earthquake, the wavenumber spectra were calculated. The observed wavenumber spectra were modeled by a two-dimensional (2D) exponential function with frequency-dependent parameters. These parameters were determined using the least squares method. Combining this 2D wavenumber spectrum model with the point power spectrum, a 3D frequency-wavenumber (FK) spectrum was obtained. This FK spectrum model was made to be non-quadrant symmetric with respect to the original wavenumber axes. Thus, the model can express propagating seismic waves having dominant directivity and velocity.

The space-time cross-spectral density function can be obtained by taking a two-fold Fourier transform of the FK spectrum. The closed form expression was sought using the two-step coordinate transform. Then the cross-spectral density function was found to be composed of two parts; i.e., a real amplitude function representing the spatial correlation and a complex phase function showing the direction and velocity of propagating waves.

The coherence function is also a common measure of space-time correlation for stochastic waves. The coherence function obtained from the FK spectrum model was compared with the two-point coherence evaluated from recorded motions. Agreement between them was found to be good.

Since only one earthquake event observed by the Chiba array was used in this paper, further studies are necessary before a more general statement on spatial variation of earthquake ground motion can be made.

REFERENCES

Abrahamson, N.A. and Bolt, B.A. 1987. Chapter 2: Array Analysis and Synthesis Mapping of Strong Seismic Motion. *Seismic Strong Motion Synthetics.* Edited by Bolt, B.A. Academic Press.

Bolt, B.A., Tsai, Y.B.,Yeh, K. and Hsu, M.K. 1982. Earthquake Strong Motions Recorded by a Large Near-Source Array of Digital Seismographs. *Earthquake eng. struct. dyn.* 10: 561-573.

Deodatis, G., Shinozuka, M. and Papageorgiou, A. 1990a. Stochastic Wave Representation of Seismic Ground Motion. I: F-K Spectra. *J. eng. mech.* 116: 11, 2363-2379. ASCE.

Deodatis, G., Shinozuka, M. and Papageorgiou, A. 1990b. Stochastic Wave Representation of Seismic Ground Motion. II: Simulation. *J. eng. mech.* 116: 11, 2381-2399. ASCE.

Harada, T. 1991. Seismic Response of Stochastic Ground. *Computational Stochastic Mechanics*: 649-660. Edited by Spanos, P.D. and Brebbia, C.A. Computational Mechanics Publications.

Harichandran, R.S. and Vanmarcke, E.H. 1986. Stochastic Variation of Earthquake Ground Motion in Space and Time. *J. eng. mech.* 112: 2, 154-174.

Katayama, T., Yamazaki, F., Nagata, S., Lu, L. and Türker, T. 1990. A Strong Motion Database for the Chiba Seismometer Array and its Engineering Analysis. *Earthquake eng. struct. dyn.* 19: 1089-1106.

Loh, C.H. 1985. Analysis of the Spatial Variation of Seismic Waves and Ground Movements from SMART-1 Array Data. *Earthquake eng. struct. dyn.* 13: 561-581.

Türker, T., Yamazaki, F. and Katayama, T. 1991. Simulation of Earthquake Ground Motion Based on Frequency-Wavenumber Spectrum. *Trans. of the 11th SMiRT* K1: 21-26.

Vanmarcke, E. 1983. *Random Fields.* Cambridge, MA: MIT Press.